Acta Geotechnica (2022) 17:93–104
https://doi.org/10.1007/s11440-021-01232-7

RESEARCH PAPER

An experimental study on the time-dependent behavior of crushable granular materials using 3D-printed particles

Ming Xu[1] · Dehai Jin[1] · Wenxuan Zhou[1]

Received: 9 August 2020 / Accepted: 4 May 2021 / Published online: 22 May 2021

Abstract

This paper aimed to investigate the potential capability of using 3D-printed particles to study the time-dependent behavior of a typical crushable granular material, i.e., rockfill. Different 3D printing techniques were compared, and gypsum powder and binder were chosen for printing crushable particles, which were found to have a comparable peak strength, ductility, and failure mode to those of the natural rockfill particles in the single-particle crushing tests. Then, large oedometer creep tests were performed on the two specimens of 3D-printed particles with and without predefined inner fissures and on a third specimen of natural limestone rockfill. The vertical pressures were applied in stages on each specimen, with a maximum value of 1.5 MPa. The test results showed that the patterns of creep strain development with time of the two specimens with 3D-printed particles were consistent with that observed for natural rockfill. The main modes of particle breakage for all three specimens after the test were asperity breakage and surface abrasion, while global fracture was not substantial. The predefined inner fissure in the 3D-printed particles only had a minor influence on the creep behavior of the specimen even at high vertical pressures. Compared with the limestone rockfill specimen, the specimens with 3D-printed particles showed similar creep behavior at low vertical pressures but exhibited much larger creep strain at high vertical pressures. The underlying mechanism of the observed phenomenon was explored.

Keywords 3D printing · Creep · Crushable granular materials · Micro-mechanism · Particle breakage mode

1 Introduction

Crushable granular materials, such as rockfills and carbonate sands, have received increasing attention in the recent decades in geotechnical engineering practice [6, 24, 25]. Even strong silica sand particles will break if the stress level is high enough [18, 28]. Crushable granular materials exhibit many complex mechanical properties, e.g., a nonlinear strength envelope, stress-dependent shearing contraction and dilatancy [1, 19, 29, 30, 33, 37]. Furthermore, crushable granular materials also exhibit time-dependent behavior, which might lead to excessive long-term settlement of high embankments, dams, and pile foundations, and thus has been receiving increasing attention [13, 14, 32, 39–41]. These time-independent behavior and time-dependent behavior are believed to be related to particle breakage [4, 5, 15–17, 36, 38].

The macro-response of crushable granular materials subjected to different loading conditions has been investigated extensively during previous laboratory studies, and the particle breakage was usually examined by measuring the particle size distribution before and after the test (e.g., [9, 31, 35]. A deeper understanding of the micro-mechanism of the observed phenomenon is desired. However, it is difficult to quantify the fundamental behavior at the particle level through conventional laboratory testing. Nakata et al. [23] performed triaxial tests on Aio sand, in which a small number (9–21) of colored quartz particles were placed in the specimen so that the breakage modes of those marked particles could be examined after the test. A similar approach was adopted in their oedometer tests on

✉ Ming Xu
mingxu@mail.tsinghua.edu.cn

Dehai Jin
jindehai1991@qq.com

Wenxuan Zhou
zwx18@mails.tsinghua.edu.cn

[1] Department of Civil Engineering, Tsinghua University, Beijing 100084, China

sand [22]. Some researchers used artificial particles in order to minimize uncertainties caused by variations in the shapes and properties of natural granular materials. Tapias et al. [27] carried out oedometer tests on sugar cubes to investigate the particle breakage mode. Takei et al. [26] performed compression creep tests on chalk bars, talc bars, and glass beads. Clearly, the particle shape and strength of these artificial particles were substantially different from those of natural particles. Zhang et al. [42, 43] performed large triaxial tests on specimens of cement ellipsoid aggregates, which were produced with similar particle strengths as those of natural rockfill particles. However, the particle shape had to be highly simplified.

In recent years, the three-dimensional printing technique has rapidly developed in mechanical engineering, which could also become a potentially powerful tool for studying geomaterials. Ishutov et al. [11] produced 3D-printed cubic samples to simulate sandstone with various patterns of porosity, in which two materials were used in printing, i.e., melted plastic filament and liquid photopolymer. Head and Vanorio [10] utilized photo-reactive resin to print cylinder samples to investigate the influence of different rock microstructures on the permeability. Jiang et al. [12] printed cylinder and block samples to study the mechanical behavior of rock with joints. They also used two materials, including polylactic acid, sand powder and blinder. Fereshtenejad and Song [7] performed uniaxial compression tests on 3D-printed cylinder samples, which were produced using powder and blinder technique.

However, rock samples were simulated in most reported studies using 3D printing techniques, while granular materials were seldom simulated. Hanaor et al. [8] printed resin particles with a size of approximately 2 mm and then performed triaxial tests on samples consisting of particles with different particle shapes. Uncrushable granular particles and instant loading were considered in this study. There was no reported research using 3D printing techniques to study the time-dependent behavior of crushable granular particles.

This paper aims to investigate the potential capability of using 3D-printed particles to study the creep behavior of a typical crushable granular material, i.e., rockfill. 3D printing technique has the advantage of producing particles with identical shape and material properties, while a certain particle feature can be designed as variable so that its influence can be studied without introducing variation in other factors. In this study, suitable 3D printing techniques and materials are identified first to produce crushable particles. Then, large oedometer creep tests are performed on the two specimens of 3D-printed particles with and without predefined inner fissures and on a third specimen of natural limestone rockfill. The mode of the particle breakage of these three specimens is examined. The influence of the predefined inner fissure in the 3D-printed particles on the global creep behavior is investigated. Furthermore, the creep behavior of the specimens with 3D-printed particles is compared with that of the limestone rockfill specimen, and the underlying mechanism of the observed phenomenon is explored.

2 3D printing methods and materials

Since there was no reported research using 3D-printed particles to simulate crushable granular particles, it was deemed necessary to first identify suitable 3D printing methods and materials. In this investigation, two 3D printing methods and related materials were adopted to print rockfill particles, which were then subjected to single-particle crushing tests and the results were compared.

2.1 3D printing methods and materials

The first method was to utilize photo-reactive resin (VisiJet M3 Crystal) by means of a ProJet 3510 SD printer. The MultiJet (MJP) 3D printing technique was used to print the particle in thin layers, each of which was hardened by UV lamps. The layer thickness was 0.03 mm. According to the production specification, the resin had a density of 1.02 g/cm^3, a tensile strength of 42.4 MPa, and a tensile modulus of 0.146 GPa. The tensile strain at breakage was 6.83%.

The second method utilized a ProJet 660Pro printer using the powder-ink binder (PIB) technique. The layer thickness was 0.1 mm. Different materials were tested to achieve properties that were similar to those of rockfills, and finally, gypsum powder and a specially designed binder (GYD-01) were chosen. A cylinder sample with a diameter of 50 mm and a height of 100 mm was printed, and the density was measured as 1.45 g/cm^3. Uniaxial compression test was performed on the cylinder sample, which revealed an unconfined compressive strength of 5.20 MPa and a Young's modulus of 1.39 GPa.

Since the printing technique involved a layer-by-layer construction process, possible anisotropy in the mechanical behavior was investigated. Two disk-shaped samples with a diameter of 50 mm and a thickness of 20 mm were printed using gypsum powder and binder. Brazilian test was performed on the first sample with the layer direction perpendicular to the loading direction and on the second sample with the layer direction parallel to the loading direction. The results showed a tensile strength of 1.16 MPa for the first sample and 1.08 MPa for the second sample, which indicated that the effect of anisotropy induced by the printing process was insignificant.

It can be seen that the 3D-printed material using gypsum powder and binder has mechanical properties that are comparable to those of some weak sandstone, e.g., Sherwood sandstone [3].

2.2 Single-particle crushing test

Three natural limestone rockfill particles were scanned to produce 3D-printed particles using the two methods described above (i.e., photo-reactive resin and gypsum powder-binder). Photographs of these three groups of particles are shown in Figs. 1a–c. The prototype natural limestone particle is placed at the center of each photograph, while the 3D-printed resin particles (in yellow color) are placed on the right side and the 3D-printed powder-binder particles (in white color) are placed on the left side. It can be seen that, in each group, the 3D-printed particles have almost identical shape as that of the corresponding prototype particle.

Single-particle crushing test was performed on each particle with a loading rate of 0.2 mm/min. Figure 2 shows the force–displacement relationships for the three groups of particles. In each group, the resin particles exhibited a peak strength that was 3–5 times higher than that of the limestone particle, and the resin particles were able to sustain very large deformations, indicating that they had a very strong ductility. In contrast, the powder-binder particles exhibited a peak strength that was approximately 30–50% lower than that of the limestone particles. The powder-binder particles reached their peak strength at a displacement of approximately 0.5–1.5 mm, which was also comparable to that for the limestone particles (approximately 1 mm).

The failure mode was examined. Both the limestone particles and the powder-binder particles fractured into two or more pieces. It is interesting to note that the limestone particles always crushed suddenly, while the gypsum powder-binder particles usually broke in a gentler manner. This can also be interpreted from the force–displacement relationships in Fig. 2. For the limestone particles, there was always a sudden drop in the force after the peak strength. For the gypsum powder-binder particles in Fig. 2a, b, the force decreased more gently with increasing displacement after reaching the peak strength, and the residual force even increased further. However, the two gypsum powder-binder particles in Fig. 2c also exhibited a sudden drop in the force.

In contrast, the resin particles experienced large plastic compressive deformations at the end of the test, although several local fissures occurred.

In conclusion, compared with the natural rockfill particles, the 3D-printed resin particles were too ductile and too difficult to break. The 3D-printed gypsum powder-binder particles had a comparable peak strength, ductility, and failure mode to those of the natural rockfill particles in the crushing test. Thus, the gypsum powder-binder particles were deemed more suitable to simulate natural rockfill particles and were adopted in the following large oedometer creep tests.

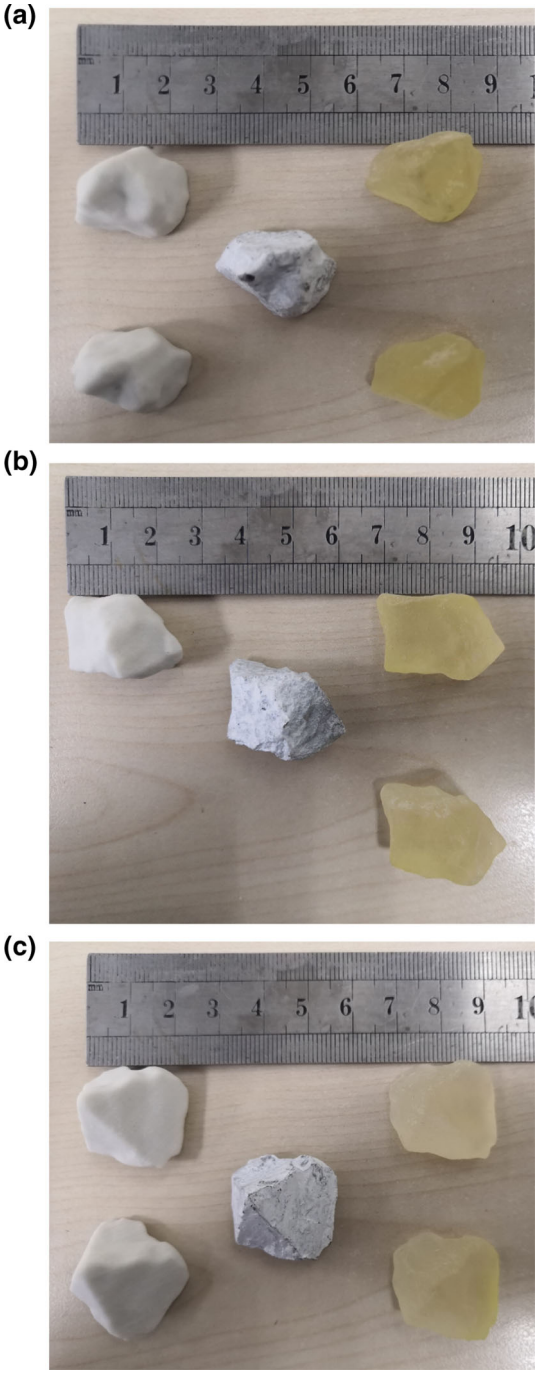

Fig. 1 Photographs of prototype natural particles and 3D-printed particles: **a** Shape 1; **b** Shape 2; **c** Shape 3. In each photograph, the natural particle is at the center, with the 3D-printed resin particles on the right and the 3D-printed powder-binder particles on the left

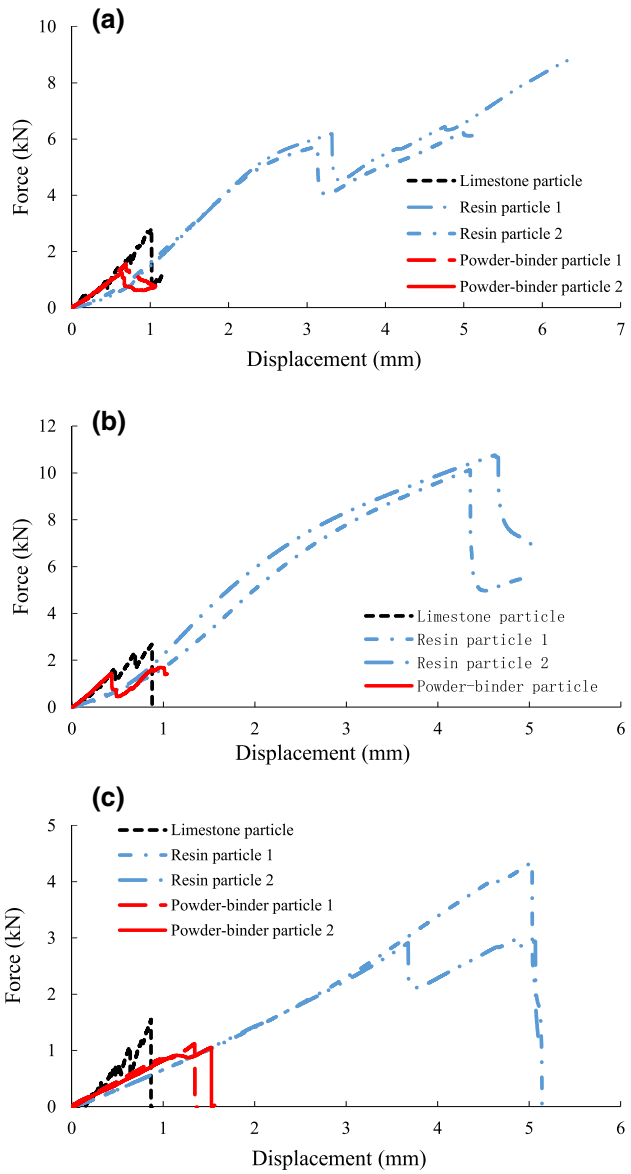

Fig. 2 The force–displacement relationship of single-particle crushing test: **a** Shape 1; **b** Shape 2; **c** Shape 3

3 Oedometer creep test procedure

3.1 Particles

A total of three specimens were tested. Specimen 1 consisted of 3D-printed gypsum powder-binder particles with identical shapes, which were printed according to the 3D-scanning shape of the same prototype rockfill particle. The particle dimensions are shown in Fig. 3a.

The micro-mechanism of the observed creep behavior of granular materials was usually attributed to the propagation of cracks inside the particle [2, 17]. Oldecop and Alonso [24] proposed a theoretical model, in which a disk-shaped particle with a pre-existing central crack was loaded diametrically. The relationship between time to breakage of the crack and its initial length was established, based on which the creep strain development of a granular assembly was derived. Therefore, Specimen 2 was designed to investigate the influence of pre-existing inner fissures in the particle. Each particle was printed with a predefined inner fissure, as shown in Fig. 3b. The length of the fissure was 10 mm, i.e., half of the maximum length of the particle. The 3D-printed particles in Specimen 2 had exactly the same particle shape as that in Specimen 1.

Specimen 3 consisted of natural limestone rockfill particles. Since Specimens 1 and 2 had 3D-printed particles with a maximum dimension of 20 mm, the rockfill particles in Specimen 3 were chosen to have maximum dimensions within the range of 16–26 mm. The particle shapes were also chosen to be as close to that of the 3D-printed particles as possible. However, a large variation in the particle shape was inevitable for the natural rockfill.

The 3D-printed particles were printed in two colors (i.e., white and gray) to facilitate observation, as shown in Fig. 3c, d. The natural limestone rockfill particles were covered with a thin layer of white paint.

3.2 Oedometer apparatus

A one-dimensional oedometer apparatus was designed, which had an inner horizontal dimension of 100 mm × 100 mm and an inner height of 130 mm, as shown in Fig. 4. The inner surfaces were lubricated to minimize friction by a thin layer of Vaseline. To permit the observation of the movement and breakage of the particles during loading, this oedometer apparatus was equipped with a thick transparent Plexiglas window on the front wall. The load was applied and maintained through a WDW-20kN universal test machine with a load capacity of 20 kN and an accuracy of 0.1%, which was controlled automatically by a computer.

3.3 Test procedure

Each specimen was prepared in four equal layers and compacted gently using a hand hammer to achieve a void ratio that was as close as possible to the specified value. Care was taken to not break the particles during preparation. The details of the three specimens are summarized in Table 1.

The testing procedure was identical for each specimen. The vertical pressure was applied stage by stage on each specimen, i.e., 0.25 MPa, 0.5 MPa, 1.0 MPa, and 1.5 MPa. At each stage, the vertical pressure was kept constant for 120 min for creep, after which the vertical pressure was increased to a higher level. The measured settlement after the first minute of loading was taken as the creep

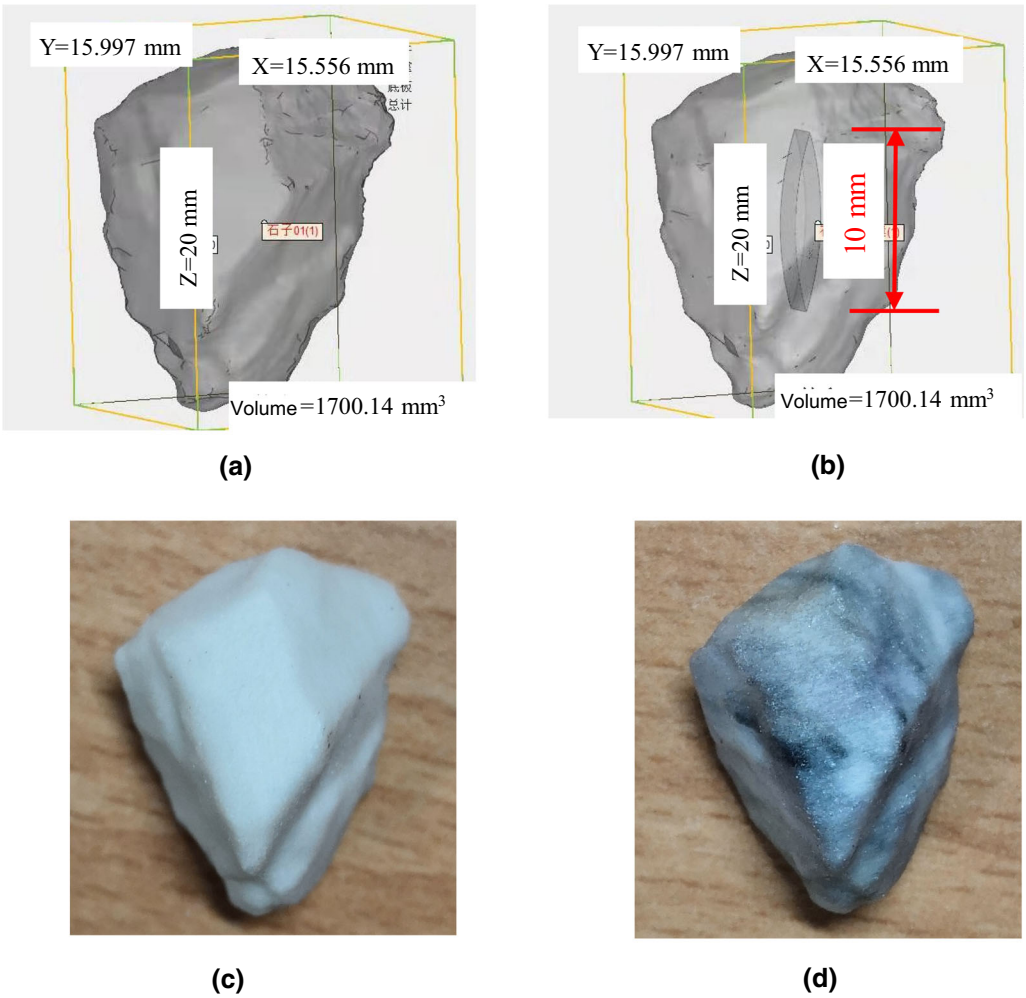

Fig. 3 The 3D-printed particles for oedometer test: **a** particle without predefined inner fissure; **b** particle with predefined inner fissure; **c** particle with white color; **d** particle with gray color

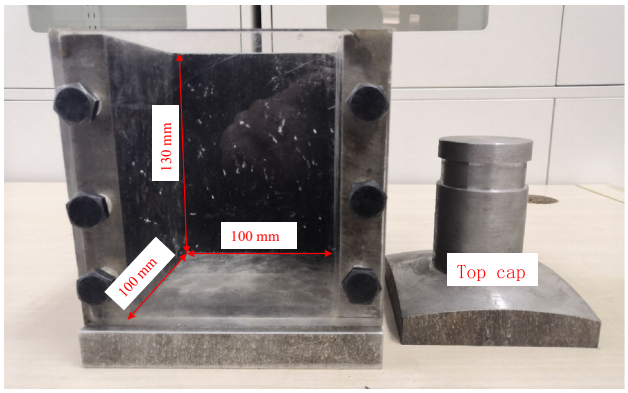

Fig. 4 The oedometer apparatus

settlement. During the test, digital photographs were frequently taken at a fixed position in front of the observation window. The maximum pressure (1.5 MPa) was approximately equal to the vertical pressure at the bottom of a 75 m high rockfill embankment.

4 Results and discussion

4.1 Creep settlement

The development of creep strain with time under different applied vertical pressures for the three specimens is plotted in Figs. 5, 6 and 7. Figures 5a, 6a, and 7a plot the time in the natural coordinates. All three specimens exhibited similar patterns of creep behavior from a qualitative point of view. The creep strain developed at a decreasing rate with increasing time, and a higher vertical pressure led to a larger creep at the end of 120 min.

Figures 5b, 6b, and 7b plot the time in the logarithmic coordinates. After the initial 10 min, an approximately linear relationship became obvious between the creep strain and the logarithm of the time for the three specimens. The slope increased with increasing vertical pressure, which was consistent with previous experimental observations for rockfill specimens [34]. Compared with the

Table 1 Parameters of the three specimens

	Specimen 1 (3D-printed uniform particles)	Specimen 2 (3D-printed particles with fissures)	Specimen 3 (limestone rockfill)
Number of particles	400	400	349
Particle density (g/cm^3)	1.45	1.45	2.7
Specimen height (mm)	110.1	109.9	110.1
Specimen horizontal dimensions (mm^2)	100 × 100	100 × 100	100 × 100
Specimen density (g/cm^3)	0.908	0.910	1.670
Void ratio	0.597	0.593	0.617

smooth curves of Specimens 1 and 2 (3D-printed particles), the curves of Specimen 3 (natural rockfill) were more uneven. Loud sounds due to particle crushing were heard during the loading of Specimen 3, the time of which were found to be associated with the fluctuations in the curve, as shown in Fig. 7c.

A quantitative comparison of the creep strains for the different specimens will be made in Sects. 4.3 and 4.4.

4.2 Particle breakage mode

The transparent front window of the oedometer allowed direct observations of the particles adjacent to the window during the test. At pressure levels of 0.25 MPa, 0.5 MPa and 1.0 MPa, no particle breakage was observed through the front window during the load application and subsequent creep period for all three specimens. The immediate settlement and creep settlement were found to be associated with the slippage and rotation of the particles.

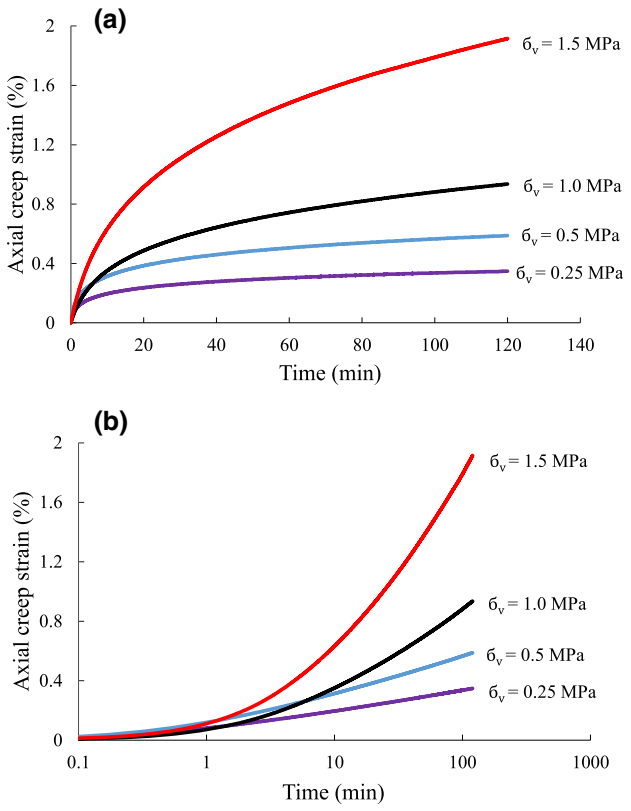

Fig. 5 Axial creep strain against time at different vertical pressures for Specimen 1 (3D-printed uniform particles): **a** time in natural coordinate; **b** time in logarithmic coordinate

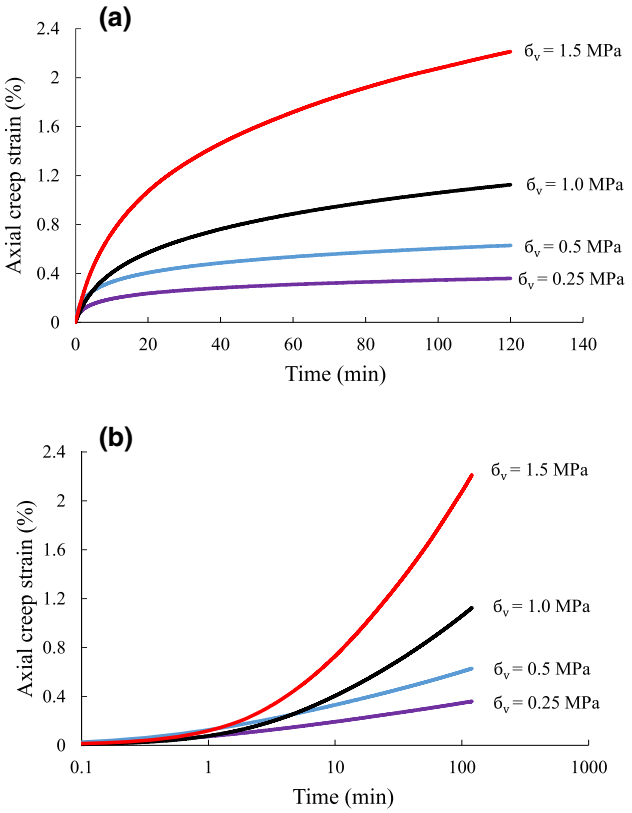

Fig. 6 Axial creep strain against time at different vertical pressures for Specimen 2 (3D-printed particles with predefined fissures): **a** time in natural coordinate; **b** time in logarithmic coordinate

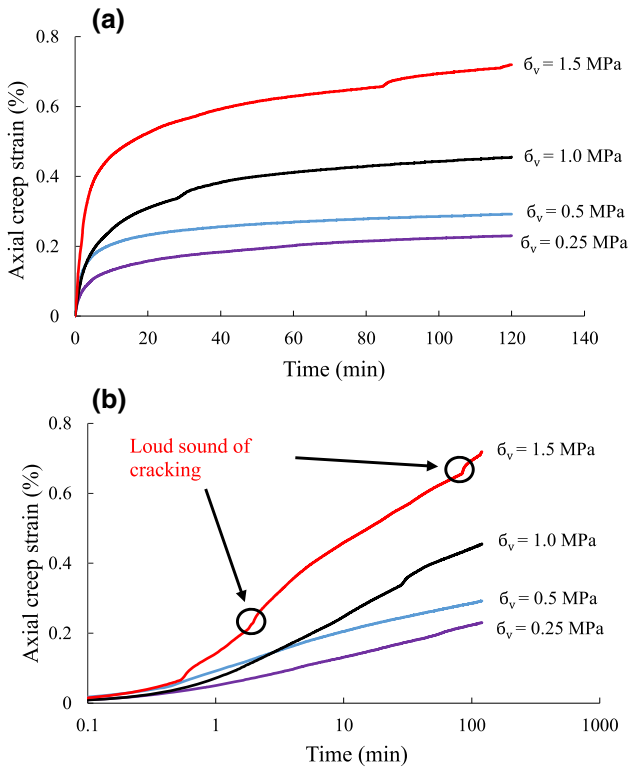

Fig. 7 Axial creep strain against time at different vertical pressures for Specimen 3 (limestone rockfill particles): **a** time in natural coordinate; **b** time in logarithmic coordinate

Figures 8, 9 and 10 show the observations for the three specimens subjected to the vertical pressure of 1.5 MPa at time t = 0, 3, and 120 min. High-resolution figures can be downloaded from: https://cloud.tsinghua.edu.cn/f/d76eb103343f46e6a98f/

For Specimen 1 (Fig. 8), the instant loading caused a vertical crack on the particle on the top-left side of the window (in the red circle). Then, this crack developed with time (as shown at t = 3 min) and finally split the particle (as shown at t = 120 min). Another crack appeared on a particle near the center (in the red rectangle) during creep, as shown at t = 120 min.

For Specimen 2 (Fig. 9), a small corner was broken off from a particle on the mid-left side of the window during instant loading (in the red circle, as shown at t = 0 min). During the creep period, a splitting crack appeared on a particle near the center at t = 3 min (in the red rectangle) and developed, as shown at t = 120 min.

For Specimen 3 (Fig. 10), the instant loading caused a small crack on the corner of a particle in the red circle (as shown at t = 0 min). The width of this crack became progressively larger during creep. Another small crack appeared on the edge of a particle at the top (in the red rectangle) during creep.

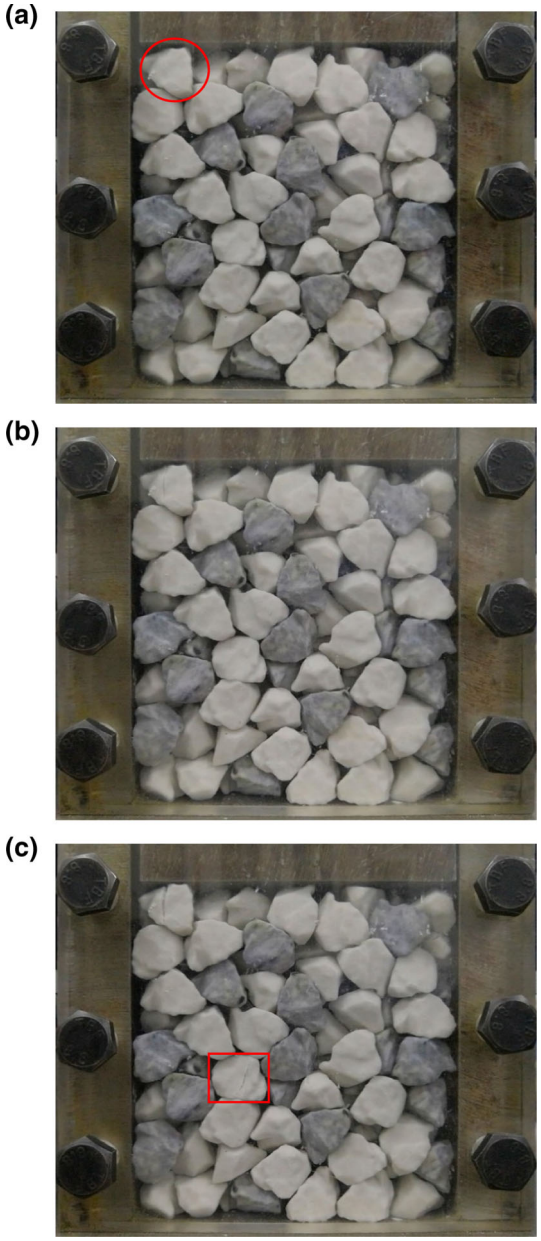

Fig. 8 Photographs of Specimen 1 (3D-printed uniform particles) under the vertical pressure of 1.5 MPa: **a** t = 0; **b** t = 3 min; **c** t = 120 min

After each test, the specimen was dissembled, and the broken particles were counted and examined. Three breakage modes were defined:

(1) Global fracture: a major fracture occurs and the original particle breaks into two or more particles.
(2) Asperity breakage: one or more corners or major asperities break off from the original particle.
(3) Surface abrasion: the particle remains whole, but there is obvious abrasion on the surface with small fines being lost.

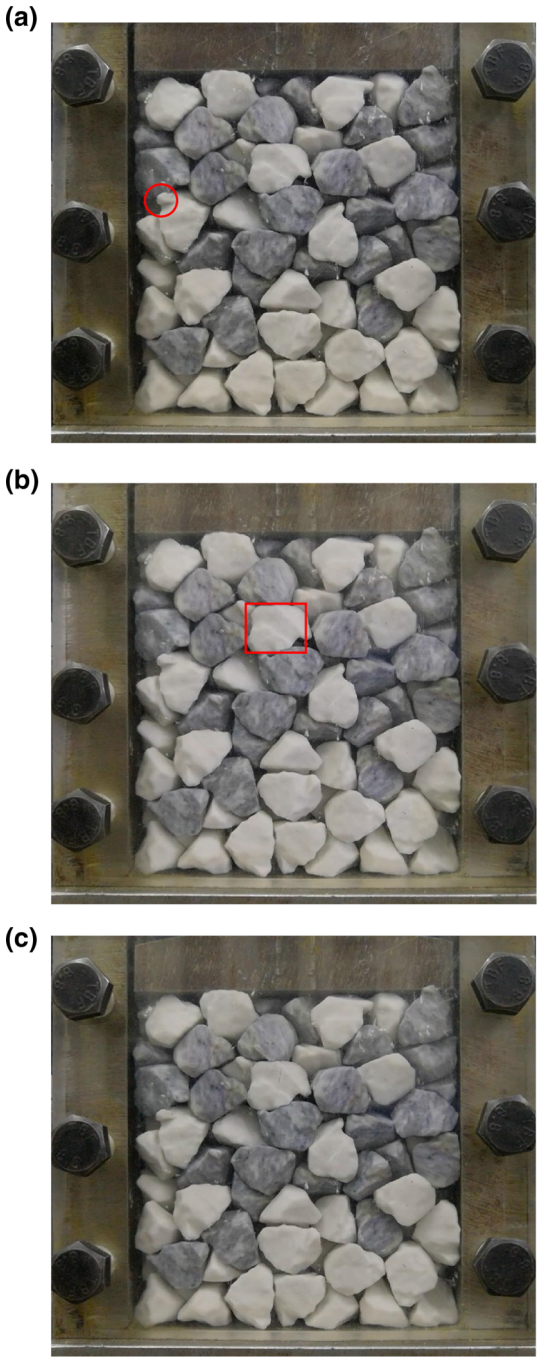

Fig. 9 Photographs of Specimen 2 (3D-printed particles with predefined fissures) under the vertical pressure of 1.5 MPa: **a** $t = 0$; **b** $t = 3$ min; **c** $t = 120$ min

The number of breakage modes is summarized in Table 2 and plotted in Fig. 11. The main modes of particle breakage for all the specimens after the test were asperity breakage and surface abrasion (with a total percentage of more than 70%), while the global fracture mode was not substantial. The high percentage of surface abrasion (approximately 50%) indicates that the slippage of particles

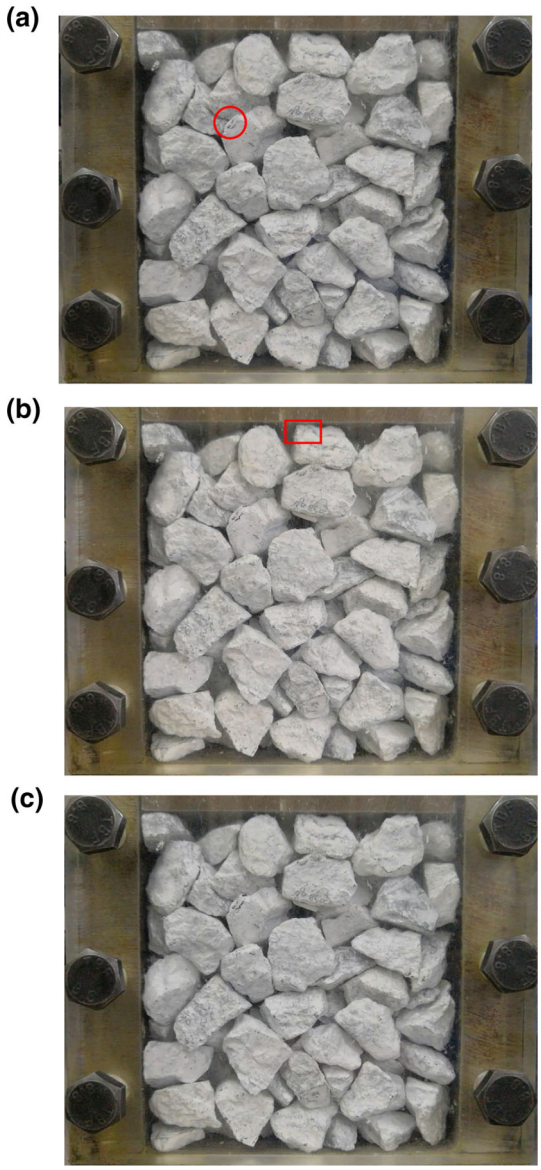

Fig. 10 Photographs of Specimen 3 (limestone rockfill particles) under the vertical pressure of 1.5 MPa: **a** $t = 0$; **b** $t = 3$ min; **c** $t = 120$ min

contributed to the deformation of the assembly. It is interesting to note that even for Specimen 2 (3D-printed particles with pre-existing inner fissure), the percentage of global fracture was only 7.3%, although this percentage was almost double that of Specimen 1 (3D-printed uniform particles), i.e., 3.8%.

In the single-particle crushing test, a particle was loaded at two points, and the breakage mode was dominantly global fracture. A pre-existing inner fissure was expected to facilitate the splitting of the particle when the fissure was oriented approximately along the loading direction. However, in the oedometer test, a particle was loaded at multiple points from the adjacent particles, as observed through

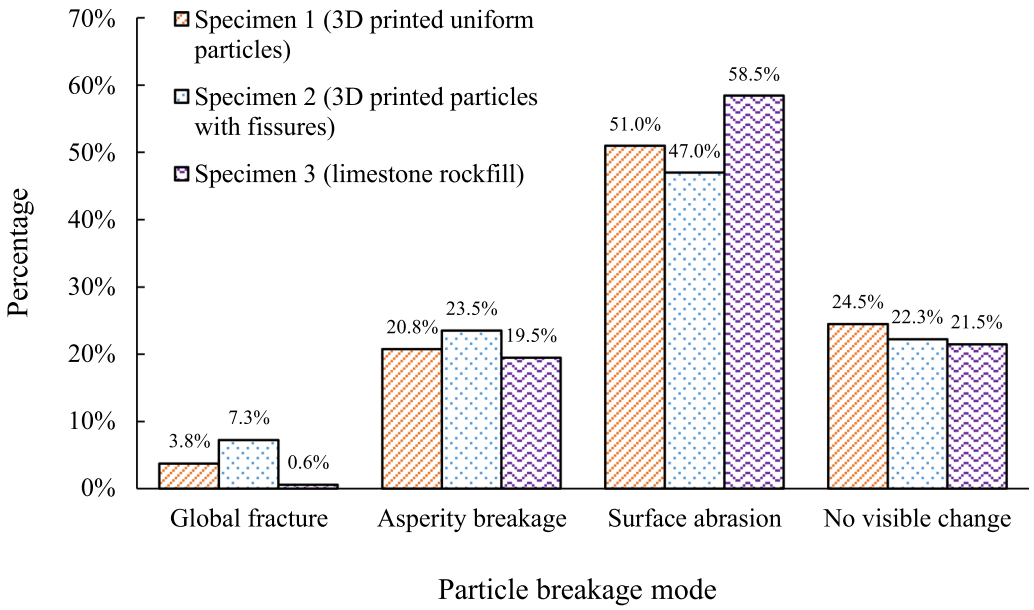

Fig. 11 Breakage modes of three specimens

the front window. In such loading conditions, asperity breakage was more likely to occur than global fracture, even there was a pre-existing inner fissure inside the particle.

Similar observation was also made by Takei et al. [26], who performed one-dimensional compression creep test under plain strain conditions on an assembly of chalk bars. The chalk bars were placed in square positions, and each bar had four contact points with the others. They also found that the main breakage pattern was asperity breakage. In contrast, the chalk bar exhibited splitting breakage during the single-particle crushing test. Xu et al. [36] simulated triaxial tests on assemblies of DEM agglomerates. Each agglomerate was made from a regular assembly of 13 spheres in hexagonal close packing. The results showed that the average coordination number of an agglomerate was approximately 10, and the dominant breakage mode was asperity breakage (i.e., 12 + 1) over a wide range of confining pressures.

4.3 Influence of pre-existing inner fissures

3D printing technology makes it possible to study the behavior of two assemblies of particles with exactly the same outer particle shape but different inner structures. Thus, the influence of inner fissures could be examined without introducing other factors, which would not have been possible if natural granular particles had been used. Figure 12 compares the development of the creep strain with the logarithm of the elapsed time for Specimen 1 (uniform particles) and Specimen 2 (particles with pre-existing inner fissures) at different vertical pressures.

At the low vertical pressures of 0.25 MPa, the two specimens exhibited almost identical creep behavior, indicating that the influence of the inner fissure was negligible. When the vertical pressure increased, Specimen 2 exhibited increasingly larger creep strain than Specimen 1. However, even at the high vertical pressures of 1.5 MPa, the difference was still small, i.e., the final creep strain was 2.2% and 1.9% for Specimen 2 and Specimen 1, respectively. Therefore, the particle inner fissure had a minor influence on the creep behavior of the assembly over the vertical pressure range investigated in this study (i.e., with a maximum value of 1.5 MPa). However, its influence is expected to increase at a higher vertical pressure.

The mechanism of the observed phenomenon can be attributed to the particle breakage mode, as discussed in Sect. 4.2. Although the number of global fractures of Specimen 2 almost doubled compared with that of

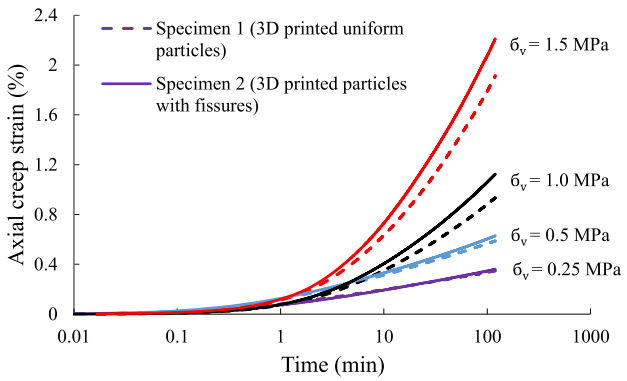

Fig. 12 The development of creep strain with time at different vertical pressures for Specimen 1 and Specimen 2

Table 2 Particle breakage modes of the three specimens

		Breakage mode			
		Global fracture	Asperity breakage	Surface abrasion	No visible change
Specimen 1	Number	15	83	204	98
	Percentage (%)	3.75	20.75	51.00	24.50
Specimen 2	Number	29	94	188	89
	Percentage (%)	7.25	23.50	47.00	22.25
Specimen 3	Number	2	68	204	75
	Percentage (%)	0.57	19.48	58.45	21.49

Specimen 1, the percentage was still low, i.e., 7.3% (Fig. 11). The major breakage modes of the particles in Specimen 2 were still asperity breakage and surface abrasion, and the pre-existing inner fissure did not lead to a large increase in the number of global breakages. As a result, the predefined inner fissures in the particles had an insignificant effect on the creep behavior of the assembly on the macro-scale.

The observations on the breakage modes have potential implications for the simulation of crushable granular particles using the discrete element method (DEM). Two techniques are usually adopted. The first is to form large agglomerates by bonding a number of elementary spheres, and the size of the latter determines the smallest fragments resulted from particle breakage (e.g., [15, 38]. Another technique is to substitute large spherical particles with a predefined number of smaller spheres (e.g., [5, 20], which inherently assumes that global fracture occurs. Although each technique has its advantages and can achieve satisfactory agreement with laboratory test results on the macro-scale, further improvement is desired.

4.4 Natural rockfill particle vs 3D-printed particles

Figure 13 plots the development of the creep strain with the logarithm of the elapsed time at the low vertical pressure (0.25 MPa) and at the high vertical pressure (1.5 MPa) for all three specimens. Figure 14 compares the final creep strains at the end of the creep periods at different vertical pressures.

At the low vertical pressure (0.25 MPa), all three specimens exhibited similar creep behavior, although the creep strain of the limestone rockfill specimen was slightly smaller than that of the other specimens. As the limestone had a higher material strength than the 3D-printed material, this also suggested that particle breakage was not the dominant mechanism of the creep deformation at low pressure levels. The observation from the front window also confirmed that the deformation was associated with particle movement (i.e., slippage and rotation) and that there was no obvious particle breakage at low pressure levels.

An increasing vertical pressure led to a larger difference between the creep strains of the specimens with 3D-printed particles and that of the rockfill specimen. At the high vertical pressure (1.5 MPa), the creep strains of Specimen 1

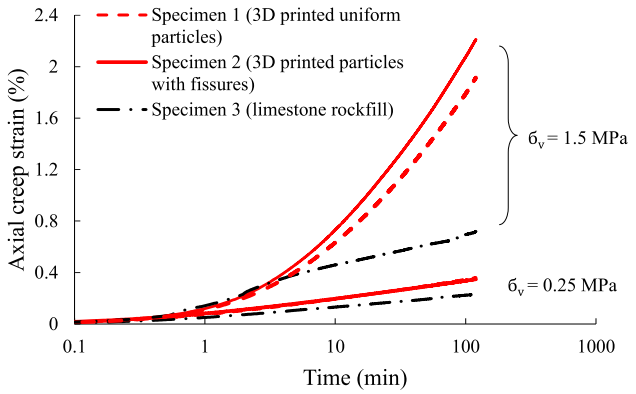

Fig. 13 The development of creep strain with time at different vertical pressures for the three specimens

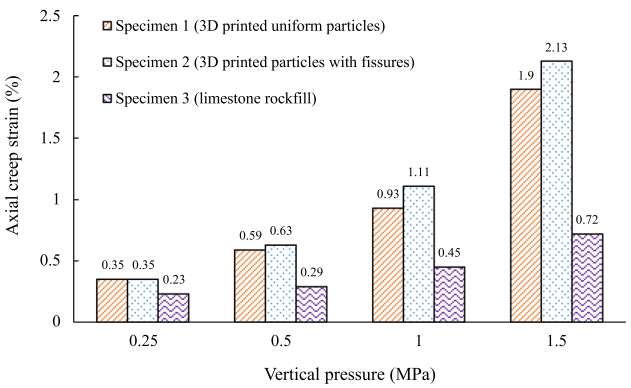

Fig. 14 Final axial creep strain at different vertical pressures for the three specimens

and Specimen 2 (3D-printed particles) were almost 3 times higher than that of Specimen 3 (limestone rockfill). Thus, at a high pressure level, the material strength had a substantial influence on the creep behavior, and the weaker particles were expected to experience more breakage. As demonstrated by Table 2 and Fig. 11, the percentage of global fracture was only 0.6% in the rockfill specimen, compared with 3.8% in Specimen 1 and 7.3% in Specimen 2.

The above observations indicate that the mechanism of the creep behavior of crushable granular materials depends on the pressure level, which can also be highlighted by comparing the findings by Michalowski et al. [21] and Lade and Karimpour [17]. Michalowski et al. [21] designed a device in which two silica sand particles were loaded with a constant force of 2.5 N. The force was applied by a spring and was small compared with the sand particle strength. Time-dependent relative movement of the two sand particles was observed, which was attributed to delayed fracturing of textural features at inter-granular contacts. In contrast, high effective confining pressure (8 MPa) was adopted by Lade and Karimpour [17] in their creep triaxial test on specimens of Virginia Beach sand. The observed creep deformation was found to be associated with significant particle crushing. However, information about particle breakage mode was not available as sieve analyses were performed.

5 Conclusion

This paper aimed to investigate the potential capability of using 3D-printed particles to study the time-dependent behavior of a typical crushable granular material, i.e., rockfill. Different 3D printing techniques were compared, and gypsum powder and binder were chosen as materials for printing crushable particles, which were found to have a comparable peak strength, ductility, and failure mode to those of the natural rockfill particles in the single-particle crushing tests. Then, large oedometer creep tests were performed on the two specimens of 3D-printed particles with and without predefined inner fissures and on a third specimen of natural limestone rockfill. The vertical pressures were applied in stages on each specimen, with a maximum value of 1.5 MPa. The test results show:

(1) The patterns of creep strain development with time of the two specimens with 3D-printed particles were consistent with that observed for natural rockfill.
(2) The main modes of particle breakage for all three specimens after the test were asperity breakage and surface abrasion, while global fracture was not substantial. This phenomenon was believed to be a result of the loading condition of the particle inside an assembly, which was more likely to be loaded at multiple points rather than two points.
(3) The predefined inner fissure in the 3D-printed particles had a minor influence on the creep behavior of the specimen over the vertical pressure range investigated in this study. However, there was a trend that its influence increased when the vertical pressure became higher.
(4) Compared with the limestone rockfill specimen, the specimens with 3D-printed particles showed similar creep behavior at low vertical pressures but exhibited much larger creep strain at high vertical pressures, which indicates that the mechanism of the observed creep behavior depends on the pressure level. At low pressure levels, the creep deformation was mainly due to particle movement (i.e., slippage and rotation). At high pressure levels, particle breakage became the dominant mechanism of the creep behavior and the material strength had a substantial influence.

This investigation highlights the advantage of using 3D-printed particles in studying the micro-mechanism, including the particle breakage mode and the influence of a specified feature (i.e., the inner fissure). In further study, more materials will be investigated so that a wide range of material strength can be achieved and different granular materials can be simulated.

Acknowledgements The authors are grateful for the research support received from the National Natural Science Foundation of China (51978382 and 41272280) and the China 973 Program (2014CB047003).

Declarations

Conflict of interest The authors declare that they have no conflict of interest.

References

1. Alhani IJ, Noor MJbM, Al-Bared MAM, Harahap ISH, Albadri WM (2020) Mechanical response of saturated and unsaturated gravels of different sizes in drained triaxial testing. Acta Geotech 15:3075–3093
2. Alonso EE, Oldecop L, Pinyol NM (2009) Long term behaviour and size effects of coarse granular media. In: Kolymbas D, Viggiani G (eds) Mechanics of natural solids. Springer, Berlin, pp 255–281
3. Bell FG (2007) Engineering geology, 2nd edn. Butterworth-Heinemann, Oxford
4. Bolton MD, Nakata Y, Cheng Y (2008) Micro- and macro-mechanical behaviour of DEM crushable materials. Géotechnique 58(6):471–480
5. de Bono JP, McDowell GR (2014) DEM of triaxial tests on crushable sand. Granular Matter 16(4):551–562

6. Donohue S, Osullivan C, Long M (2009) Particle breakage during cyclic triaxial loading of a carbonate sand. Geotechnique 59(5):477–482
7. Fereshtenejad S, Song J (2016) Fundamental study on applicability of powder-based 3D printer for physical modeling in rock mechanics. Rock Mech Rock Eng 49(6):2065–2074
8. Hanaor D, Gan Y, Revay M, Airey D, Einav I (2016) 3D printable geomaterials. Geotechnique 66(4):323–332
9. Hardin BO (1985) Crushing of soil particles. J Geotech Eng 111(10):1177–1192
10. Head D, Vanorio T (2016) Effects of changes in rock microstructures on permeability: 3-D printing investigation. Geophys Res Lett 43:7494–7502
11. Ishutov S, Hasiuk F, Harding C, Gray JN (2015) 3D printing sandstone porosity models. Interpretation 3(3):SX49
12. Jiang Q, Feng X, Song L, Gong Y, Zheng H, Cui J (2016) Modeling rock specimens through 3D printing: tentative experiments and prospects. Acta Mech Sin 32(1):101–111
13. Kermani M, Konrad JM, Smith M (2017) An empirical method for predicting post-construction settlement of concrete face rockfill dams. Can Geotech J 54(6):755–767
14. Kong Y, Xu M, Song E (2017) An elastic-viscoplastic double-yield-surface model for coarse-grained soils considering particle breakage. Comput Geotech 85:59–70
15. Kwok CY, Bolton MD (2013) DEM simulations of soil creep due to particle crushing. Geotechnique 63(16):1365–1376
16. Lade PV, Yamamuro JA, Bopp PA (1996) Significance of particle crushing in granular materials. J Geotech Eng 122(4):309–316
17. Lade PV, Karimpour H (2010) Static fatigue controls particle crushing and time effects in granular materials. Soils Found 50(5):573–583
18. Leung CF, Lee FH, Yet NS (1996) The role of particle breakage in pile creep in sand. Can Geotech J 33(6):888–898
19. Liu H, Zou D (2012) Associated generalized plasticity framework for modeling gravelly soils considering particle breakage. J Eng Mech 139(5):606–615
20. Lobo-Guerrero S, Vallejo LE, Vesga LF (2006) Visualization of crushing evolution in granular materials under compression using DEM. Int J Geomech 6(3):195–200
21. Michalowski RL, Wang Z, Nadukuru SS (2018) Maturing of contacts and ageing of silica sand. Géotechnique 68(2):133–145
22. Nakata Y, Hyodo M, Hyde AF, Kato Y, Murata H (2001) Microscopic particle crushing of sand subjected to high pressure one-dimensional compression. Soils Found 41(1):69–82
23. Nakata Y, Hyde AFL, Hyedo M, Murata H (1999) A probabilistic approach to sand particle crushing in the triaxial test. Géotechnique 49(5):567–583
24. Oldecop LA, Alonso EE (2007) Theoretical investigation of the time-dependent behaviour of rockfill. Geotechnique 57(3):289–301
25. Orense RP, Pender MJ, Hyodo M, Nakata Y (2013) Micro-mechanical properties of crushable pumice sands. Geotechnique Letters 3(2):67–71
26. Takei M, Kusakabe O, Hayashi T (2001) Time-dependent behavior of crushable materials in one-dimensional compression tests. Soils Found 41(1):97–121
27. Tapias M, Alonso EE, Gili JA (2016) Compressibility, grain breakage and time-dependent behavior of gap-graded aggregates of sugar cubes. Soils Found 56(5):805–817
28. Randolph M, Dolwin J, Beck RD (1994) Design of driven piles in sand. Geotechnique 44(3):427–448
29. Varadarajan A, Sharma KG, Abbas SM, Dhawan AK (2006) Constitutive model for rockfill materials and determination of material constants. Int J Geomech 6(4):226–237
30. Xiao Y, Liu H, Chen Y, Jiang J, Zhang W (2014) State-dependent constitutive model for rockfill materials. Int J Geomech 15(5):04014075
31. Xiao Y, Liu H, Desai CS, Sun Y, Liu H (2016) Effect of intermediate principal-stress ratio on particle breakage of rockfill material. J Geotech Geoenviron Eng 142(4):06015017
32. Xiao Y, Yuan Z, Desai CS, Zaman M, Ma Q, Chen Q, Liu H (2020) Effects of load duration and stress level on deformation and particle breakage of carbonate sands. Int J Geomech 20(7):06020014
33. Xu M, Song E (2009) Numerical simulation of the shear behavior of rockfills. Comput Geotech 36(8):1259–1264
34. Xu M, Song E, Cao G (2009) Compressibility of broken rock-fine grain soil mixture. Geomech Eng 1(2):169–178
35. Xu M, Song E, Chen J (2012) A large triaxial investigation of the stress-path-dependent behavior of compacted rockfill. Acta Geotech 7(3):167–175
36. Xu M, Hong J, Song E (2017) DEM study on the effect of particle breakage on the macro- and micro-behavior of rockfill sheared along different stress paths. Comput Geotech 89:113–127
37. Xu M, Song E, Jin D (2017) A strain hardening model for the stress-path-dependent shear behavior of rockfills. Geomech Eng 13(5):743–756
38. Xu M, Hong J, Song E (2018) DEM study on the macro- and micro-responses of granular materials subjected to creep and stress relaxation. Comput Geotech 102:111–124
39. Xu M, Jin D, Song E, Shen D (2018) A rheological model to simulate the shear creep behavior of rockfills considering the influence of stress states. Acta Geotech 13:1313–1327
40. Xu M, Jin D, Song E, Shen Z, Yang Z, Fu J (2019) Full-scale creep test and back-analysis of the long-term settlement of heavy-loaded shallow foundations on a high rockfill embankment. Comput Geotech 115:103156
41. Yao Y, Huang J, Wang N, Luo T, Han L (2020) Prediction method of creep settlement considering abrupt factors. Transp Geotech 22:100304
42. Zhang B, Jie Y, Kong D (2013) Particle breakage of cement ellipsoid aggregate—Part I: triaxial compression tests. J Test Eval 42(1):1–11
43. Zhang B, Jie Y, Kong D (2013) Particle breakage of cement ellipsoid aggregate—Part II: investigation of particle crushing. J Test Eval 41(5):1–9